Journal of Power Sources 274 (2015) 41–47

Contents lists available at ScienceDirect

Journal of Power Sources

journal homepage: www.elsevier.com/locate/jpowsour

Specific considerations for obtaining appropriate $La_{1-x}Sr_xGa_{1-y}Mg_yO_{3-\delta}$ thin films using pulsed-laser deposition and its influence on the performance of solid-oxide fuel cells

Jaeyeon Hwang [a, b], Heon Lee [b], Jong-Ho Lee [a, c], Kyung Joong Yoon [a, c], Hyoungchul Kim [a], Jongsup Hong [a], Ji-Won Son [a, c, *]

[a] High-Temperature Energy Materials Research Center, Korea Institute of Science and Technology, Seoul 136-791, Republic of Korea
[b] Department of Materials Science and Engineering, Korea University, Seoul 136-701, Republic of Korea
[c] Nanomaterials Science and Engineering, Korea University of Science and Technology, KIST Campus, Seoul 136-791, Republic of Korea

HIGHLIGHTS

- Exact transfer of the composition of the LSGM target to the film is not possible.
- Target composition control and a high deposition temperature are necessary.
- An SOFC with an optimized LSGM thin-film electrolyte yielded 1.1 W cm^{-2} at 600 °C.

GRAPHICAL ABSTRACT

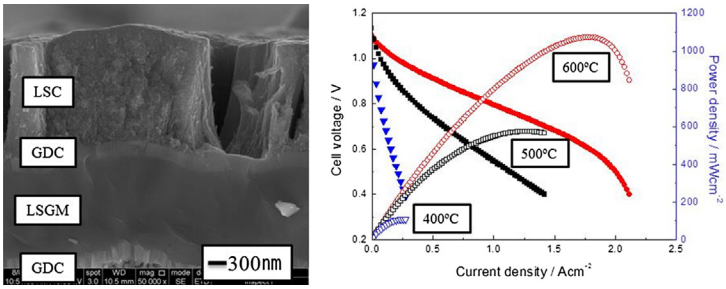

ARTICLE INFO

Article history:
Received 28 July 2014
Received in revised form
2 October 2014
Accepted 3 October 2014
Available online 12 October 2014

Keywords:
Sr- and Mg-doped $LaGaO_3$
Thin-film electrolyte
Pulsed-laser deposition
Solid-oxide fuel cell
Composition transfer

ABSTRACT

To obtain $La_{1-x}Sr_xGa_{1-y}Mg_yO_{3-\delta}$ (LSGM) thin films with the appropriate properties, pulsed-laser deposition (PLD) is employed, and specific considerations regarding control of the deposition parameters is investigated. It is demonstrated that with a target of stoichiometric composition, appropriate LSGM thin films cannot be produced because of the deviation of the composition from the target to the thin film. Only after adjusting the target composition an LSGM thin film with an appropriate composition and phase can be obtained. The optimized LSGM thin film possesses an electrical conductivity close to that of the bulk LSGM. In contrast, non-optimized thin films do not yield any measurable electrical conductivity. The impact of the optimization of the LSGM thin-film electrolyte on the cell performance is quite significant, in that a solid-oxide fuel cell (SOFC) with an optimized LSGM thin-film electrolyte produces a maximum power density of 1.1 W cm^{-2} at 600 °C, whereas an SOFC with a non-optimal LSGM thin-film electrolyte is not operable.

1. Introduction

A solid-oxide fuel cell (SOFC) is an electrochemical device that has the potential to produce much more electricity than other competing technologies. The typical operating temperatures of conventional SOFC systems are 800–1000 °C [1]. Such high operating temperatures lead to problems, such as limitations in material

* Corresponding author. High-Temperature Energy Materials Research Center, Korea Institute of Science and Technology, Hwarangno 14-gil 5, Seongbuk-gu, Seoul 136-791, Republic of Korea. Tel.: +82 2 958 5530; fax: +82 2 958 5529.
E-mail address: jwson@kist.re.kr (J.-W. Son).

http://dx.doi.org/10.1016/j.jpowsour.2014.10.023
0378-7753/

selections, high fabrication costs, and the inability to apply SOFCs as portable power sources. Therefore, research has erred toward lower the operating temperatures below 500–600 °C [1,2].

To gain higher performance with low-temperature-operating SOFCs (LT-SOFCs), a new electrolyte that has a higher ionic conductivity at lower temperature and stability in both reducing and oxidizing atmospheres is required. Doped zirconias, such as yttria-stabilized zirconia (YSZ), are the most common electrolyte material and are sufficiently stable under a wide range of oxygen partial pressures (pO_2). Nevertheless, the ionic conductivity of zirconia-base electrolytes is relatively poor for applications in LT-SOFCs compared with other promising electrolyte materials [3]. On the other hand, doped ceria materials, such as Gd-doped ceria (GDC), are strong candidates as electrolytes in LT-SOFCs because they have a higher ionic conductivity and lower activation energy (E_a). Doped ceria materials, however, exhibit n-type semiconduction in a reducing atmosphere, which consequentially causes a drop in the open circuit voltage (OCV) [3]. For these reasons, Sr- and Mg-doped $LaGaO_3$ ($La_{1-x}Sr_xGa_{1-y}Mg_yO_{3-\delta}$: LSGM) materials have gained a good deal of attention as alternative electrolyte materials. An appropriate doping level ($0.1 \leq x \leq 0.2$, $0.15 \leq y \leq 0.25$) provides advantages for LSGMs, such as stability in various atmospheres and sufficient ionic conductivity to be used as an electrolyte for LT-SOFCs [4,5].

Nevertheless, LSGM has a critical problem when applied on the SOFC as an electrolyte. To fabricate LSGM while maintaining a dense microstructure and avoiding the secondary phases, the sintering temperature of the LSGM needs to be above 1400 °C [6–8]. At such high temperatures, LSGM reacts with common electrode materials in SOFCs, e.g., Ni and Ni-based cermet anode materials [9,10] as well as perovskite cathode materials [11–13]. Accordingly, for LSGM to be used as an SOFC electrolyte, the fabrication temperature should be as low as possible to suppress the formation of the secondary phases while acquiring a sufficient density in the microstructure. Concurrently, it is also important to make a thinner electrolyte to decrease the operating temperature of the SOFC by decreasing the ohmic resistance of the electrolyte.

To solve the aforementioned issues, LSGM thin-film fabrication using pulsed-laser deposition (PLD) has been studied actively [14–17]. Despite these studies, given that the range of doping levels and fabrication temperatures that can be used to achieve the appropriate single phase of the LSGM is very small, it is hard to reliably produce LSGM thin films, even though the PLD technique is the best thin-film deposition tool for complex oxides. For this reason, many studies have presented various deposition conditions, but few were successful in realizing proper LSGM thin films. For example, in some previous studies [14,15], in spite of the fact that the LSGM thin films exhibited an appropriate electrical conductivity, they could not be applied as an electrolyte for an SOFC because of their porous microstructure. As a result, no studies were successful in building SOFCs based on the LSGM thin-film electrolyte, except for those of Ishihara et al. [17–19].

Therefore, in this study, the origin of the difficulties in realizing appropriate LSGM thin films is systematically investigated. By thoroughly characterizing the LSGM thin film from a stoichiometric target, the problems are identified in terms of the phase, crystallinity, and cation composition. Starting from this point, the specific considerations regarding control of the deposition parameters of the PLD, such as controlling target composition and substrate temperatures, needed to obtain the LSGM thin films with desired properties are determined. Comparison of the material properties such as crystallinity and electrical conductivity between optimized and un-optimized LSGM thin films is performed. The impact of these efforts on the performance of the thin-film LSGM electrolyte-based SOFCs is also tested and presented.

2. Experiments

2.1. Evaluation of the thin film deposited using the stoichiometric target

The target of the LSGM stoichiometric composition was made with a commercial LSGM powder (Seimi Chemical); its composition was $La_{0.8}Sr_{0.2}Ga_{0.8}Mg_{0.2}O_{3-\delta}$. The LSGM pellet was formed by a cold isostatic press, and the pellet was sintered at 1200 °C for 3 h. The target made with the commercial powder will be denoted as LSGM-S (S: stoichiometric) and the thin film from this target will be denoted as TF-S. A KrF excimer laser (λ = 248 nm, COMPEX Pro 201F, Coherent) was used as an ablation source for PLD. The laser fluence (energy density) at the target surface was approximately 3 J cm^{-2}, and the target-to-substrate distance was 5 cm. The thin films were deposited on c-plane sapphire (0001) or MgO (100) substrates using PLD at substrate temperatures of 700, 725, and 750 °C. The ambient O_2 pressure for deposition was 6.67 Pa.

The phase and composition were analyzed using X-ray diffraction (XRD), the selected area electron diffraction (SAED) of the transmission electron microscopy (TEM), and the energy dispersive spectroscopy (EDS) of the scanning electron microscopy (SEM). XRD indexing was performed by using a commercial software (HighScore Plus ver 3.0, PANalytical). The electrical conductivity of the thin film was measured using a 2-probe AC conductivity measurement with a Solartron impedance analyzer with an electrochemical interface (SI1260 and SI1287) at temperatures that varied from 400 to 600 °C in atmospheric air.

2.2. Adjustment of the target composition to obtain the optimal LSGM thin film

All of the experimental procedures were the same except for the powder compositions used to make the PLD targets. Different compositions of LSGM powders, La_2O_3 (99.9%, Sigma–Aldrich), $SrCO_3$ (99.5%, Cerac), Ga_2O_3 (99.9%, Kojundo), and MgO (99.9%, Kojundo) were ball-milled for one day and calcined at 1000 °C for 3 h. One of the compositions of the powder used was La:Sr:Ga:Mg = 0.7282:0.1:0.638:0.4255, which was reported by Ishihara et al. [17] to obtain the proper LSGM thin films. The other composition used was La:Sr:Ga:Mg = 0.68:0.19:0.87:0.27, which was customized for this study through trial and error. These targets will be denoted as LSGM-R (R: reference) and LSGM-C (C: customized), respectively. The thin films from each target will be denoted as TF-R and TF-C, respectively.

2.3. Comparison of the cell performances of the LSGM thin-film electrolyte-based SOFCs

After analyzing the LSGM thin films, building and testing of the SOFCs with each thin-film electrolyte was performed. 2 cm × 2 cm substrates, consisting of a NiO–YSZ anode support and an anode functional layer, were fabricated by a conventional powder process. A 3 μm-thick NiO–GDC interlayer, 250 nm-thick GDC lower buffer layer, 2 μm-thick LSGM electrolyte, 250 nm-thick GDC upper buffer layer, and a 3 μm-thick $La_{0.6}Sr_{0.4}CoO_{3-\delta}$ cathode layer were stacked on the substrate using PLD with the optimal deposition conditions for each component, which have been established in the present and previous studies by the authors [20,21]. All deposited layers except the cathode covered the entire surface of the substrate, and the area of the cathode was 1 cm × 1 cm.

A custom-made button cell test setup [20,21] was employed for the unit cell test. Air and humidified H_2 (3% H_2O) were used as the oxidant and the fuel, respectively. The flow rate on each side was kept at 200 sccm. The cell operating temperature was varied from

600 to 400 °C at 100 °C intervals, and the impedance spectra (IS) at the open circuit voltage (OCV) and current-voltage-power (*I–V–P*) curves were obtained at each temperature. An Iviumstat analyzer was used to obtain IS and *I–V–P* curves, and each IS was observed at a frequency range from 10 MHz to 0.1 Hz. After the cell test, microstructures of each cell were characterized using SEM.

3. Results and discussion

3.1. Evaluation of the thin film deposited using the stoichiometric target

Fig. 1 shows the XRD patterns of the LSGM-S target, the TF-S deposited at 700 °C (labeled as 700 °C), deposited at room temperature and post-annealed (PA) at 700 °C for 1 h (labelled as R.T. 700 °C PA), and deposited at 750 °C, respectively (labelled as 750 °C). The LSGM-S exhibited proper diffraction peaks from the LSGM phase. Unlike the commonly used electrolytes, such as YSZ and GDC that are easily grown with fair crystallinity at 700 °C [22], the TF-S deposited at 700 °C did not show any XRD diffraction peaks, which indicates that it is amorphous. In the case of the TF-S deposited at room temperature and annealed at 700 °C, the major phase was $La_4Ga_2O_9$, which is an A-site-rich perovskite. The XRD pattern of the TF-S deposited at 750 °C reveals that although the film is crystalline, it is not a single LSGM phase, but many other secondary phases that cannot be indexed that exist. This result indicates that single-phase LSGM thin films cannot be produced using the LSGM-S at the present conditions.

These results could also be confirmed with the TEM analyses shown in Fig. 2. Fig. 2(a) and (b) shows a typical amorphous image and the SAED pattern, respectively, of the TF-S deposited at 700 °C. The post-annealed TF-S consisted of grains with a diameter of approximately 50 nm, as shown in Fig. 2(c). The $La_4Ga_2O_9$ phase existed, and it was identified from the complicated SAED pattern in Fig. 2(d). The TF-S deposited at 750 °C consisted of nano-sized grains (~20 nm), as seen in Fig. 2(e). The SAED pattern of the TF-S deposited at 750 °C in Fig. 2(f) also indicates many secondary phases. Usually, single-phase thin films deposited at a high substrate temperature exhibit columnar grain structures. The microstructure of the TF-S deposited at 750 °C consisting of equiaxed grains may originate from the mixture of the phases.

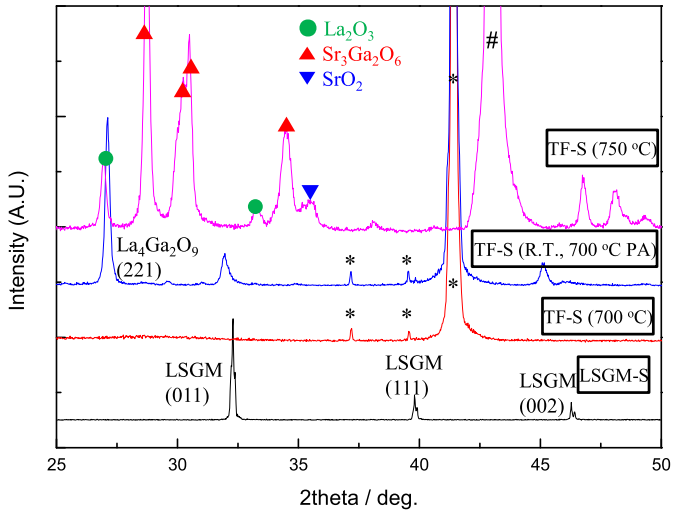

Fig. 1. XRD patterns of LSGM-S, TF-S deposited at 700 °C, TF-S deposited at room temperature and annealed at 700 °C for 1 h, and TF-S deposited at 750 °C (*: sapphire substrate, #: MgO substrate).

To seek the origin of the failure to produce the desired thin film, the compositions of the LSGM-S and the TF-S were probed by the EDS and listed in Table 1. Unlike the target that shows a proper composition, the TF-S turns out to have the ratio of La:Sr:Ga:Mg = 0.95:0.20:0.69:0.16, which shows a lack of B-site cations, such as Ga and Mg. This result was consistent with the phase analyses by the XRD and TEM results. Based on these results, it is supposed that the deficiency of the B-site cations in the TF-S affects the formation of secondary phases such as $La_4Ga_2O_9$. Because $La_4Ga_2O_9$ is a resistive phase, the electrical conductivity of the TF-S is expected to be low.

Because the composition of the thin film deviates from the correct stoichiometry, it is impossible to produce proper LSGM thin films by varying the deposition conditions, post-deposition treatments, and so on. Ju et al. also reported a similar phenomenon, and proposed that it originated from the difference between the vapor pressures of the elements [16]. Another possible cause of this phenomenon is the differential scattering in the plume [23,24]. This is plausible because previous PLD studies on PLD-deposited films with the stoichiometric target were performed under relatively high working pressures [15] or under a high vacuum [14], which can homogenize scattering in the plume [23,24]. Adjusting working pressure especially to high working pressures, however, is not an acceptable approach for solving this problem because the microstructure of the thin film becomes porous, thereby making it ill-suited as the microstructure of the electrolyte. To obtain the LSGM thin film with the correct stoichiometry and phase without losing the dense microstructure due to a deposition pressure change, the target composition needed to be adjusted.

3.2. Adjustment of the target composition to obtain the optimal LSGM thin film

The thin-film deposition with the LSGM-R (target from Ref. [17]) was tried first, and the composition of the TF-R was confirmed by EDS. After integration of the two results (the composition of the TF-S and TF-R) along with several other experiments, the loss of the B-site cations, Ga and Mg, was observed. This was balanced by adding more B-site cations to the target composition. The optimized target composition was determined to be La:Sr:Ga:Mg = 0.68:0.19:0.87:0.27.

For comparison of the composition of the customized LSGM targets and thin films, EDS data of these are listed in Table 2. According to these data, it is demonstrated again that exact transference of the cation composition from the target to the thin film is obstructed. From the viewpoint of the A:B cation ratio, the TF-R show a deficiency of the B-site cations. Comparing TF-R and TF-C, the composition of TF-R was not consistent with the results from [17], though the substrate temperature and ambient pressure were altered similar values as used in their study. This result demonstrates that for complex materials such as LSGM, the thin film production conditions can be significantly different depending on the apparatus and environment. This is thought to be the reason why it is such a challenge to obtain desirable LSGM thin films.

In Fig. 3, the XRD patterns of the TF-C and the LSGM-C are displayed. The TF-C shows good crystallinity, and there is little of the secondary phase present (possibly MgO). One interesting observation is that the LSGM-C does not have the proper LSGM phase. In spite of that, an LSGM thin film of the appropriate phase was obtained by using the LSGM-C, contrary to the case that used the LSGM-S. Therefore, it is postulated that for some cases with complex oxides, a non-stoichiometric target can be more favorable to obtain the thin film with the right composition and phase, though it does not possess the exact phase in question. Again, the crystallinity of the film was confirmed by TEM. The TF-C showed a

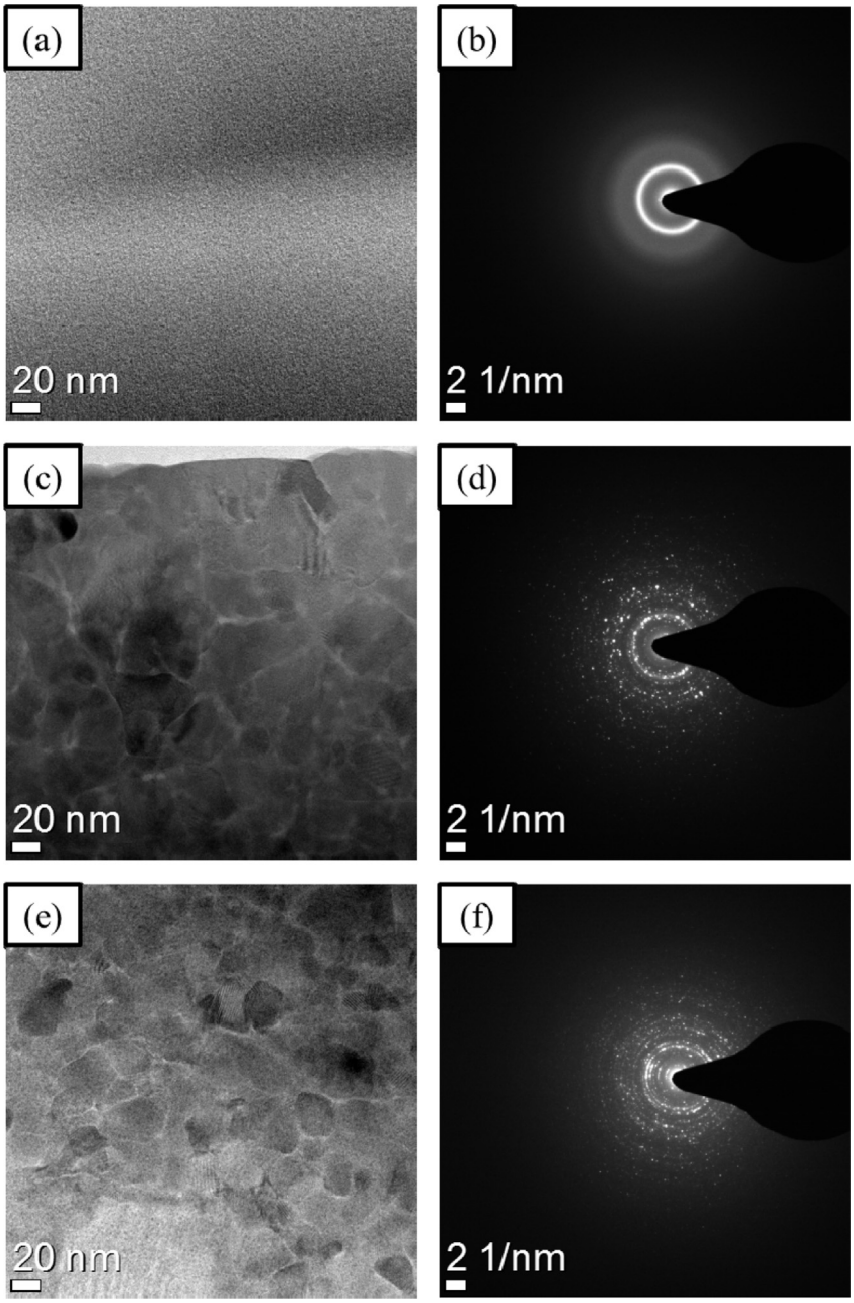

Fig. 2. Bright-field TEM images and SAED patterns of (a, b) TF-S deposited at 700 °C, (c, d) TF-S deposited at room temperature and annealed at 700 °C for 1 h, and (e, f) TF-S deposited at 750 °C.

well-crystallized structure as seen in Fig. 4(a). The SAED pattern of a grain could be indexed as (100) plane of $La_{0.8}Sr_{0.2}Ga_{0.8}Mg_{0.2}O_{3-\delta}$ (ICSD 98-009-8170), as shown in Fig. 4(b). This implies that the right composition of the thin film is the key to obtain the proper phase, crystallinity, and structure of the thin film.

Table 1
EDS results of LSGM-S and TF-S deposited at 750 °C (unit is converted to atomic percent for each perovskite site).

(Atomic %)	La	Sr	Ga	Mg	A-site	B-site	A:B
LSGM-S	80	20	80	20	100	100	1
TF-S	94.78	20.38	68.78	16.06	115.2	84.8	1.357

The thin film examined in Fig. 3 was deposited at a substrate temperature of 750 °C for comparison with the last TF-S deposited with the LSGM-S in the Section 3.1. As previously mentioned, lower deposition temperature is preferable in terms of the deposition

Table 2
EDS results of customized LSGM targets and LSGM thin films made with each target at 750 °C (unit is converted to atomic percent for each perovskite site).

(Atomic %)	La	Sr	Ga	Mg	A-site	B-site	A:B
LSGM-R	72.82	10	63.8	42.55	82.8	106.4	0.779
TF-R	94.02	11.74	58.04	36.2	105.8	94.2	1.122
LSGM-C	68	19	87	27	87	114	0.763
TF-C	83.73	19.64	83.21	13.42	103.4	96.6	1.07

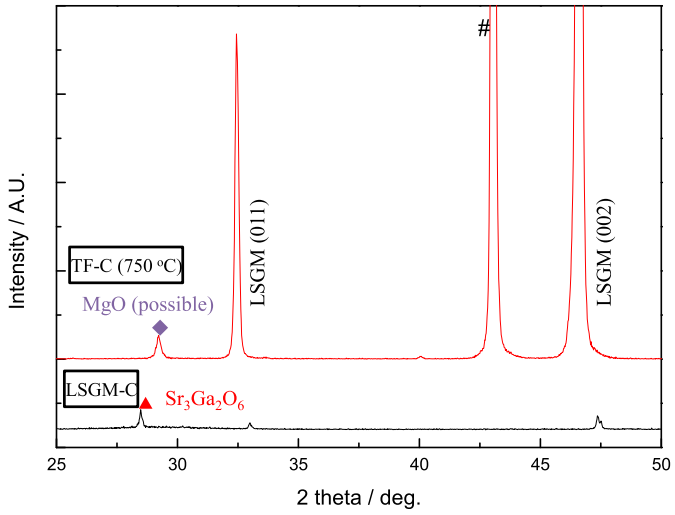

Fig. 3. XRD patterns of LSGM-C and TF-C deposited at 750 °C (#: MgO substrate).

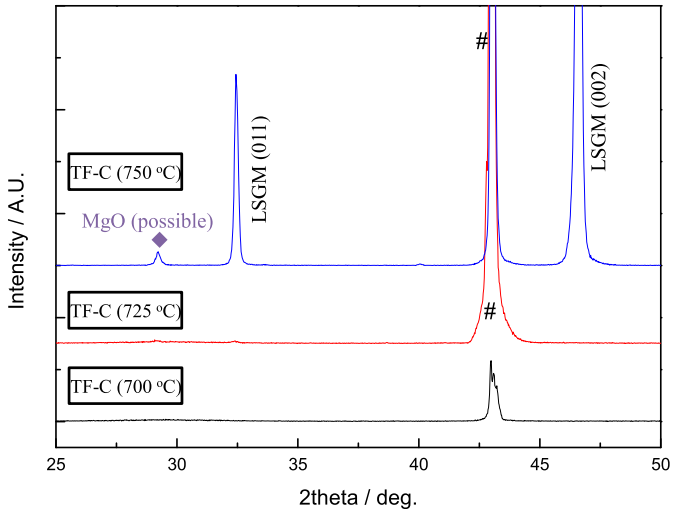

Fig. 5. XRD patterns of TF-C deposited in various temperatures (#: MgO substrate).

system requirements and the prevention of the chemical reaction. Therefore, deposition temperatures lower than 750 °C were tried, and as shown in Fig. 5, the diffraction peaks from the LSGM phase disappeared when the deposition temperature was below 750 °C. These results demonstrate that LSGM thin films still require a higher deposition temperature than that of electrolytes with simpler compositions, such as YSZ and GDC (~700 °C was sufficient for these materials). It is thought that not only the composition optimization but also the higher substrate temperature are required for the crystallization of the LSGM thin film. These results clearly show the challenges associated with obtaining the appropriate LSGM thin film, and special consideration should be given for successful realization of an LSGM thin film.

The electrical conductivity of the thin films was measured, and an Arrhenius plot of the electrical conductivity of the optimized TF-C is given in Fig. 6. The TF-C deposited at 750 °C exhibits an electrical conductivity close to that of the bulk LSGM and the activation energy (E_a) of the conductivity of the thin film ($E_a = 1.020 \pm 0.013$ eV) is also similar to that of the bulk. For other non-optimized thin films in the present study, the TF-Cs deposited at lower temperatures and the TF-Ss, the resistance was too high so the conductivity could not be estimated with the given measurement setup. This shows that the optimization of the LSGM thin film in terms of the composition, and thus the phase, crystallinity and structure, should be satisfied to obtain the proper electrical properties of the LSGM thin films.

3.3. Comparison of the cell performances of the LSGM thin-film electrolyte-based SOFCs

To investigate the impact of the LSGM thin film optimization, both TF-S and TF-C were applied to a thin-film electrolyte-based SOFC (TF-SOFC) platform and cell performance was measured. As shown in the IS graph of Fig. 7, the Cell-S (the cell with TF-S electrolyte) shows very high resistance. The scattering of the data is caused by an unstable OCV. The cell performance of the Cell-S could not be tested at all tested temperatures. Meanwhile, the Cell-C (the cell with TF-C electrolyte) shows much improved cell performances in Fig. 8, which is similar to that of the state-of-art YSZ thin-film electrolyte-based cell seen in the previous study by authors [21]. Ohmic area specific resistances (ASR_{ohm}), polarization area specific resistances (ASR_{pol}), OCVs, and power densities of the Cell-C at 400, 500, and 600 °C are listed in Table 3. The ASRs are deduced from the Nyquist plots of the cell, and the OCVs as well as the power densities are obtained from the *I–V–P* curves of the cell given in Fig. 8. The results demonstrate that the optimization of the LSGM thin film is essential to obtain proper cell performance based on the LSGM thin-film electrolyte.

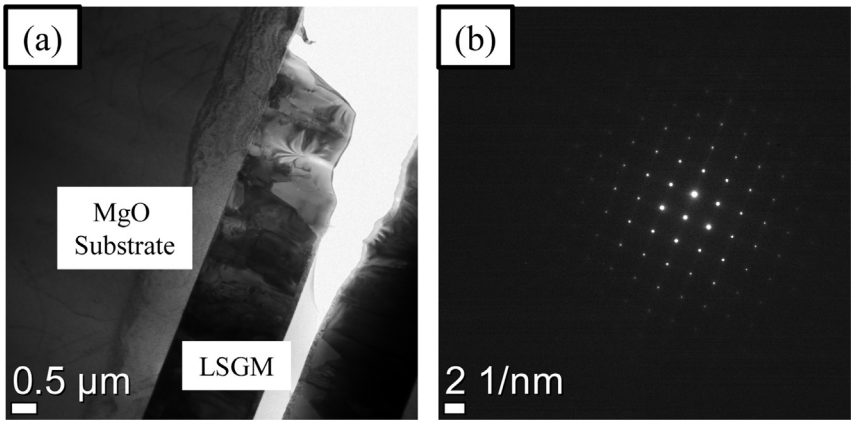

Fig. 4. (a) Bright-field TEM image and (b) SAED patterns of TF-C deposited at 750 °C.

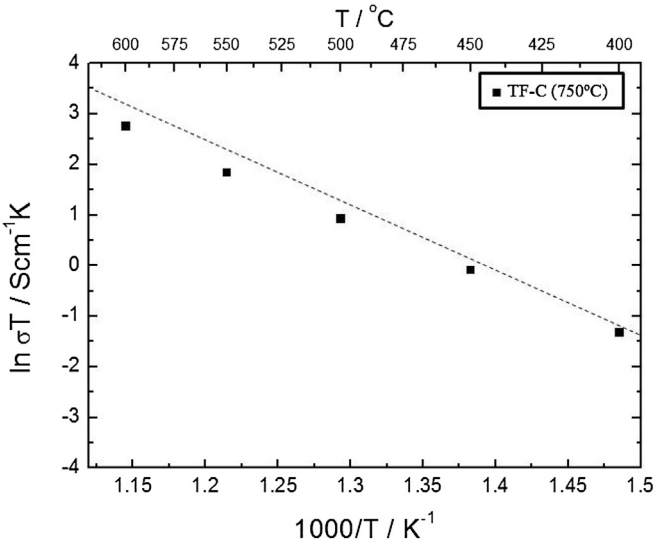

Fig. 6. Arrhenius plot of the electrical conductivity of TF-C deposited at 750 °C (dotted line: bulk Ref. [25]).

The cell performance in the present study is compared with the previous results from the LSGM thin-film electrolyte-based SOFCs from the Ishihara group [17–19]. According to Ref. [18], the maximum power density of the cell of Ref. [18] (will be denoted as Cell-REF1) was 1951 mW cm^{-2} at 600 °C, and it was approximately two times higher than that of the Cell-C. This performance difference seems to originate from the difference in the cell configurations and operating conditions. While the ASR_{ohm} values of each cell are in a similar range, the ASR_{pol} of the Cell-REF1 was 0.100 Ω cm^2 and that of the Cell-C was 0.794 Ω cm^2 at 600 °C. This large difference is considered to stem from the electrochemical performance of the different electrodes of the cells, as well as from the gas composition used during operation. Another study from the same group reports that the maximum power density of the cell (Cell-REF2) is approximately 1000 mW cm^{-2} at 600 °C, which was similar to that of the Cell-C [19]. Because Cell-REF1, Cell-REF2, and Cell-C employed highly active Co-containing perovskite cathodes ($(Sm,Sr)CoO_{3-\delta}$ for Cell-REF1, 2 and $(La,Sr)CoO_{3-\delta}$ for Cell-C), it is postulated that the difference of the anode material may be the main reason for the cell performance differences among the three cases, and the quality of the LSGM thin film electrolyte of the present study is not far-off from that of the cases used for comparison.

After the cell test, the microstructure of Cell-C was observed; the SEM micrograph of the cross-section is shown in Fig. 9. Both in low-magnification (Fig. 9(a)) and high-magnification (Fig. 9(b)), there is no visible defect in the interior of the LSGM electrolyte, or at the interfaces between the electrolyte and the buffer layers at top and bottom of the electrolyte. The material compatibility of the LSGM electrolyte with adjacent components is thought to be secured based on this observation.

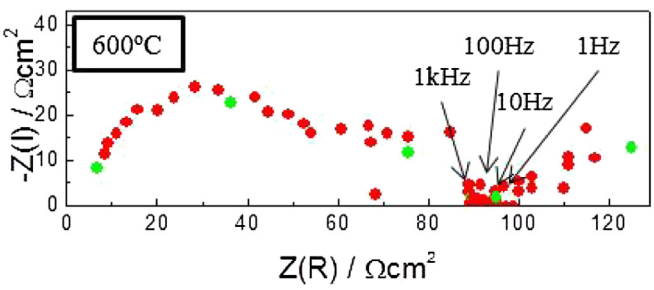

Fig. 7. IS graph of the Cell-S measured at 600 °C, OCV.

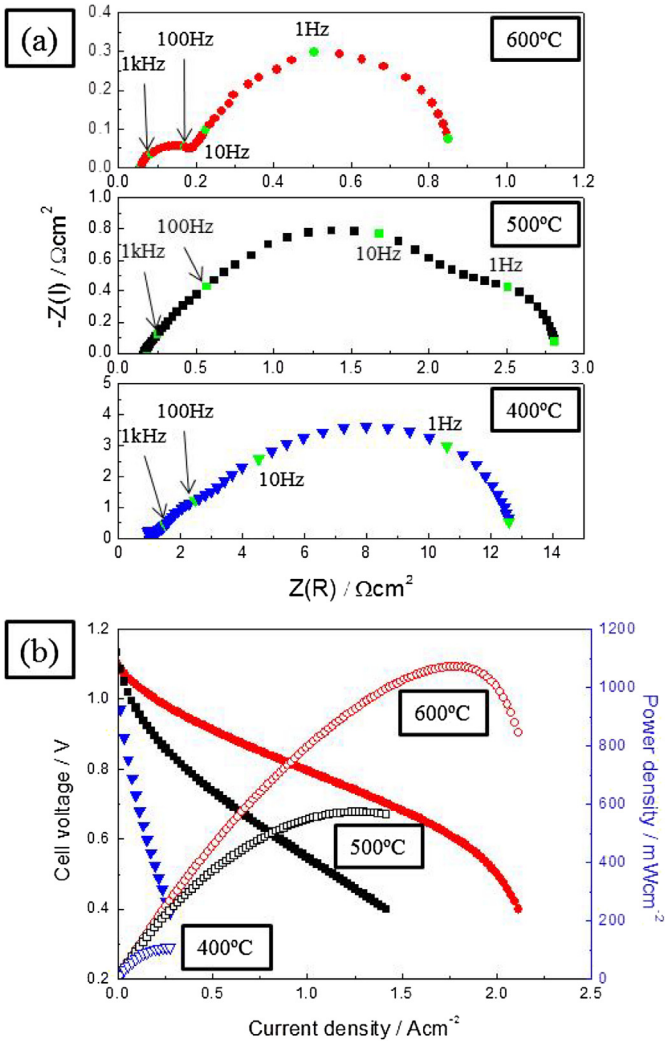

Fig. 8. (a) IS and (b) *I–V–P* curves of the Cell-C at various temperatures.

4. Conclusions

The origin of the difficulties in realizing appropriate LSGM thin films was investigated by studying the LSGM thin films produced using PLD with stoichiometric and customized targets. It is demonstrated that exact transference of the cation composition from the target to the thin film is obstructed, and the deviation of the thin-film composition from the correct stoichiometry causes the amorphization and/or generation of the secondary phases. It is also shown that intentional deviation of the target cation composition from stoichiometric conditions is essential to obtain the proper composition of the thin film and that thin film production conditions can be significantly different depending on the apparatus and the environment. In terms of the deposition temperature, over 750 °C is necessary for crystallization of the LSGM thin film, which indicates that it is more difficult to obtain the crystallinity of the LSGM thin film compared with cases using electrolyte thin films

Table 3
Ohmic ASR, polarization ASR, OCV, peak power density, and power density at 0.7 V of the Cell-C at each temperature.

Temperature (°C)	Ohm. ASR at OCV (Ω cm^2)	Pol. ASR at OCV (Ω cm^2)	OCV (V)	Power density at 0.7 V (mW cm^{-2})	Peak power density (mW cm^{-2})
600	0.057	0.794	1.097	997	1073
500	0.168	2.643	1.121	414	573
400	1.177	11.591	1.143	74	108

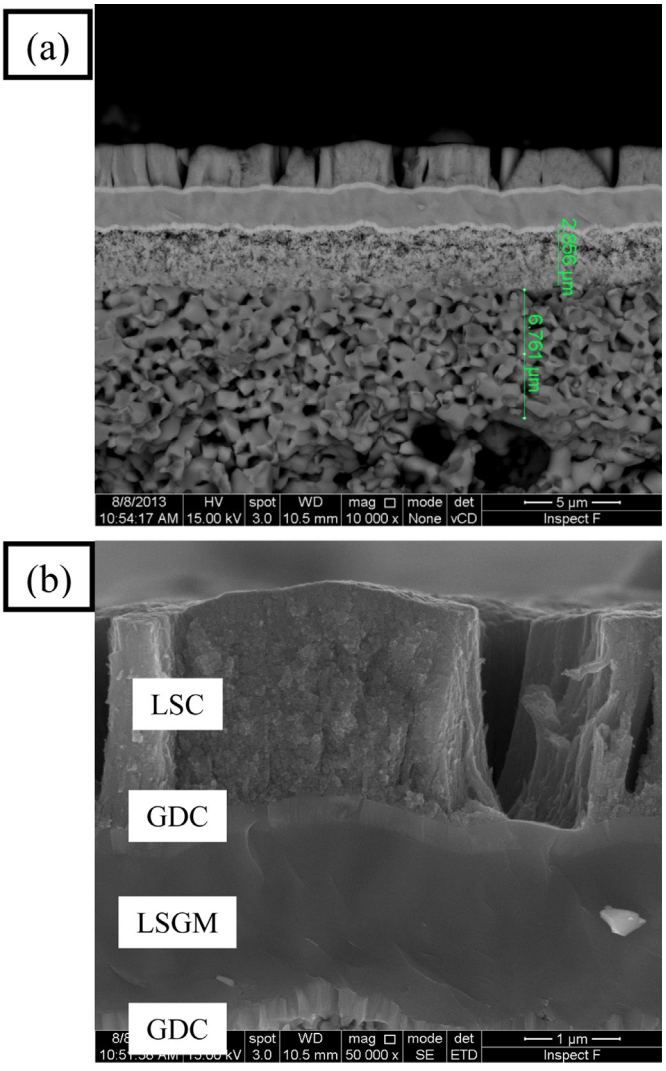

Fig. 9. (a) Low-magnification and (b) high-magnification cross-sectional microstructure of the Cell-C after cell test.

of simpler compositions. The optimized LSGM thin film shows a high electrical conductivity, which is comparable to that of the bulk LSGM. The cell with the optimized LSGM thin-film electrolyte yielded a decent cell performance, whereas the cell with the non-optimized LSGM did not. Therefore, optimization of the LSGM thin film is a prerequisite to obtaining proper performance of LSGM thin-film electrolyte-based SOFCs.

Acknowledgments

The authors would like to thank Dr. Young-Wan Ju (Kyushu Univ., UNIST) for valuable discussions. This work was financially supported by the Young Fellow Program of KIST and the Global Frontier R&D Program on Center for Multiscale Energy Systems (2011-0031579) funded by the National Research Foundation under the Ministry of Science, ICT & Future Planning, Korea.

References

[1] D. Beckel, A. Bieberle-Hutter, A. Harvey, A. Infortuna, U.P. Muecke, M. Prestat, J.L.M. Rupp, L.J. Gauckler, J. Power Sources 173 (2007) 325–345.
[2] D.H. Myung, J. Hwang, J. Hong, H.W. Lee, B.K. Kim, J.H. Lee, J.W. Son, J. Electrochem. Soc. 158 (2011) B1000–B1006.
[3] B.C.H. Steele, A. Heinzel, Nature 414 (2001) 345–352.
[4] T. Ishihara, H. Matsuda, Y. Takita, J. Am. Chem. Soc. 116 (1994) 3801–3803.
[5] M. Feng, J.B. Goodenough, Eur. J. Solid State Inorg. Chem. 31 (1994) 663–672.
[6] K. Huang, R.S. Tichy, J.B. Goodenough, J. Am. Ceram. Soc. 81 (1998) 2565–2575.
[7] P. Majewski, M. Rozumek, F. Aldinger, J. Alloys Compd. 329 (2001) 253–258.
[8] P. Majewski, M. Rozumek, C. Tas, F. Aldinger, J. Electroceram. 8 (2002) 65–73.
[9] P. Huang, A. Horky, A. Petric, J. Am. Ceram. Soc. 82 (1999) 2402–2406.
[10] X. Zhang, S. Ohara, R. Maric, H. Okawa, T. Fukui, H. Yoshida, T. Inagaki, K. Miura, Solid State Ionics 133 (2000) 153–160.
[11] K. Huang, M. Feng, J.B. Goodenough, M. Schmerling, J. Electrochem. Soc. 143 (1996) 3630–3636.
[12] A.T. Duong, D.R. Mumm, J. Power Sources 241 (2013) 281–287.
[13] G.C. Kostogloudis, C. Ftikos, A. Ahmad-Khanlou, A. Naoumidis, D. Stöver, Solid State Ionics 134 (2000) 127–138.
[14] P. Manoravi, N. Sivakumar, M. Joseph, T. Mathews, Ionics 10 (2004) 32–38.
[15] Y.-T. Lim, J. Son, Electron. Mater. Lett. 9 (2013) 241–243.
[16] Y.-W. Ju, H. Matsumoto, T. Ishihara, T. Inagaki, H. Eto, J. Korean Ceram. Soc. 45 (2008) 796–801.
[17] T. Ishihara, H. Eto, J.W. Yan, Int. J. Hydrogen Energy 36 (2011) 1862–1867.
[18] J.W. Yan, H. Matsumoto, M. Enoki, T. Ishihara, Electrochem. Solid State Lett. 8 (2005) A389–A391.
[19] Y.W. Ju, S. Ida, T. Inagaki, T. Ishihara, Solid State Ionics 216 (2012) 58–63.
[20] H.S. Noh, J.W. Son, H. Lee, J.S. Park, H.W. Lee, J.H. Lee, Fuel Cells 10 (2010) 1057–1065.
[21] H.-S. Noh, K.J. Yoon, B.-K. Kim, H.-J. Je, H.-W. Lee, J.-H. Lee, J.-W. Son, J. Power Sources 247 (2014) 105–111.
[22] H.S. Noh, J.S. Park, H. Lee, H.W. Lee, J.H. Lee, J.W. Son, Electrochem. Solid State Lett. 14 (2011) B26–B29.
[23] C.B. Arnold, M.J. Aziz, Appl. Phys. A 69 (1999) S23–S27.
[24] J.-W. Son, S. Orlov, B. Phillips, L. Hesselink, J. Electroceram. 17 (2006) 591–595.
[25] T. Ishihara, H. Matsuda, Y. Takita, Solid State Ionics 79 (1995) 147–151.